Remote Sensing Applications: Society and Environment 31 (2023) 100997

Contents lists available at ScienceDirect

Remote Sensing Applications: Society and Environment

journal homepage: www.elsevier.com/locate/rsase

UAV-derived photogrammetric point clouds and multispectral indices for fuel estimation in Mediterranean forests

Raúl Hoffrén [a, *], María Teresa Lamelas [a, b], Juan de la Riva [a]

[a] Geoforest-IUCA, Department of Geography and Land Management, University of Zaragoza, Pedro Cerbuna 12, 50009, Zaragoza, Spain
[b] Centro Universitario de la Defensa, Academia General Militar, Ctra. de Huesca s/n, 50090, Zaragoza, Spain

ARTICLE INFO

Keywords:
Forest fuels
Photogrammetry
Vegetation indices
GLCM
Machine learning

ABSTRACT

Sensors attached to unmanned aerial vehicles (UAVs) allow estimating a large number of forest attributes related to forest fuels. This study assesses photogrammetric point clouds and multispectral indices obtained from a fixed-wing UAV for the classification of Prometheus fuel types in 82 forest plots in Aragón (NE Spain). Images captured by an RGB camera and a multispectral sensor allowed generating high density photogrammetric point clouds (RGB: 3000 points/m^2; multispectral: 85 points/m^2), which were normalized using alternatively a Digital Elevation Model (DEM) of 0.5, 1, and 2 m resolution. A set of structural and textural variables were derived from the normalized point cloud heights, and for the latter, the gray-level co-occurrence matrix (GLCM) approach was used. Multispectral images were also used to create seven spectral vegetation indices. The most relevant structural, textural, and spectral variables to introduce into the fuel types classification models were selected using Dunn's test, which included: the vegetation height at the 50th percentile, the coefficient of variation of the heights, the percentage of returns above 4 m, the mean textural dissimilarity, and the mean of the Green Chlorophyll Index. Three different data samples were introduced in the models: i) the relevant structural and textural variables from the RGB camera (RGB data sample); ii) the relevant structural, textural, and spectral variables from the multispectral sensor (MS data sample); and iii) the relevant structural and textural variables from the RGB camera plus the relevant spectral variable from the multispectral sensor (integrated data sample). After comparing three machine learning classification techniques (Random Forest, and Linear and Radial Support Vector Machine), the best results were obtained with Random Forest with k-fold cross-validation (k-10) and the integrated data sample with normalized point clouds at 0.5 m DEM resolution (overall accuracy = 71%). The variables successfully identified the Prometheus main fire carriers (i.e., shrubs or trees) and confusions were mainly located within the fuel types of the same dominant stratum, especially in fuel types 3 and 6. These results demonstrate the ability of UAV imagery to classify forest fuels in Mediterranean environments when RGB and multispectral data are combined.

1. Introduction

Forest fires are a recurrent disturbance of Mediterranean ecosystems (Oliveira et al., 2012). Moreover, their exposure to fire may grow in the future due to the increase of wildfires globally (Varol et al., 2021; Venäläinen et al., 2020), making these ecosystems even more vulnerable. Therefore, it is essential to understand fire behavior in a forest stand in order to mitigate the detrimental ef-

* Corresponding author.
E-mail address: rhoffren@unizar.es (R. Hoffrén).

https://doi.org/10.1016/j.rsase.2023.100997
Received 20 January 2023; Received in revised form 10 May 2023; Accepted 22 May 2023
Available online 24 May 2023

fects of wildfires on the environment. Forest fuels allow estimating and quantifying fire spread over vegetation to assess fire risk and develop mitigation plans (Ferraz et al., 2016). They consist of all living or dead organic matter available for combustion in a wildfire. They are usually grouped by fuel types associated with vegetation classes that exhibit similar fire behavior. Several fuel types classifications have been developed to identify forest fuels in heterogeneous environments (e.g., Albini, 1976; Rothermel, 1972), but one specifically to Mediterranean ecosystems: The Prometheus fuel model (Prometheus, 1999), which considers vegetation height, density, and vertical continuity as the main fire spreaders and comprises seven fuel types (FT) for three main fire carriers: FT1 for grasslands; FT2, FT3, and FT4 for shrublands; and FT5, FT6, and FT7 for tree canopies. Shrub fuel types are determined by areas with more than 60% shrub cover at different mean heights, which are 0.30–0.60 m for FT2, 0.60–2 m for FT3, and 2–4 m for FT4. In terms of tree canopy types, these areas are characterized by tree cover greater than 50% at more than 4 m, with no associated understory for FT5, with a vertical difference between understory and canopies greater than 0.5 m for FT6, and with complete vertical continuity of fuels for FT7.

In last decades, remote sensing has shown great potential for estimating forest attributes and identifying forest fuels. Specifically, Airborne Laser Scanners (ALS) have been widely used because of their ability to penetrate the canopy cover and provide accurate details of forest structure, allowing for a comprehensive assessment of forest fuels. Several studies have also shown that the integration of ALS with multispectral imagery improves the identification of fuel types (e.g., Domingo et al., 2020; Marino et al., 2016). Nevertheless, few studies have used sensors on unmanned aerial vehicles (UAVs) to identify forest fuels (e.g., Fernández-Álvarez et al., 2019; Hillman et al., 2021; Shin et al., 2018), despite their ability to collect vegetation spectral response from multispectral sensors with unprecedented spatial resolution, and to estimate vegetation structure and textural features from three-dimensional point clouds. The latter can be derived directly from active sensors, such as LiDAR, or indirectly from optical images, such as RGB or multispectral sensors, through "Structure from Motion" algorithm, which is based on traditional photogrammetry (Messinger et al., 2016) using a collection of overlapping images taken from different viewpoints (Puliti et al., 2015). Although photogrammetric point clouds cannot penetrate the canopy, they can be an affordable option for estimating forest attributes over much more expensive LiDAR systems. For instance, photogrammetric point clouds were used by Fritz et al. (2013) to map tree stem in open stands, by Shin et al. (2018) to estimate fuels and forest canopy structure in a ponderosa pine stand, and by Carbonell-Rivera et al. (2022) to classify Mediterranean shrub species.

In this context, the main objective of this study is to assess the suitability of UAV-derived photogrammetric point clouds and multispectral indices for the identification of fuel types based on the Prometheus model in Mediterranean forest plots, as well as for their classification using machine learning techniques. We hypothesize that optical UAVs can be a cost-effective alternative to less affordable active sensors (such as ALS and LiDAR UAVs), as they are capable of estimating a wide range of forest attributes, including structural, textural and spectral features of vegetation using a single instrument, whereas with active sensors spectral information is lost. This capability ultimately allows the identification of forest fuels at an unprecedented detail, representing a very valuable and accessible tool to prevent and mitigate forest fires at local and regional scales in Mediterranean ecosystems.

2. Materials and methods

2.1. Study area

UAV flights were performed in 82 forest plots of 15 m of circular radius distributed in 5 sectors of the Aragón region (NE Spain) (Fig. 1), located nearby Almudévar (12 plots), Ayerbe (36 plots), Uncastillo (11 plots), Villarluengo (15 plots), and Zuera (8 plots) The average annual temperature of the entire region is 12.3 °C. All the sectors have a Mediterranean climate, but there are differences between them. The Almudévar, Ayerbe and Zuera sectors are located in the center of the Ebro Valley, characterized by very hot summers and cold winters, high daily temperature gradients, and low rainfall localized mainly in the equinoctial seasons (Almudévar: ~350 mm/year; Ayerbe: ~700 mm/year; Zuera: ~250 mm/year). The Uncastillo sector is located at the interface between the Ebro Valley and the foothills of the Pre-Pyrenean mountain range, which results in lower daily and annual thermal gradients than in the center of the valley, although still high, and mean annual rainfall of ~700 mm/year. The Villarluengo sector is placed in the Iberian mountain range, whit less hot summers and colder winters than in the other sectors due to its higher altitude, and a mean annual rainfall of ~600 mm/year. Convective storms can be frequent in late spring and summer in all sectors, but are especially important in the Villarluengo sector, where they are often accompanied by lightning that threaten the possibility of wildfires. The Prometheus fuel types for each plot were estimated in-situ in previous field work (see Montealegre et al., 2016; Domingo et al., 2020), but they were validated in each flight campaign, constituting the ground-truth for the classification models (Table 1). Plots were selected using a stratified random sampling in order to ensure a wide range of different environments (i.e., slope, exposure, vegetation cover, etc.) and, thus, fuel types. The center of the plots was located using a Leica VIVA® GS15 CS10 GNSS real-time kinematic Global Positioning System with sub-meter accuracy. Plots were mainly dominated by grassland, shrublands, and forest of Aleppo pine (*Pinus halepensis* Mill.) and bog pine (*Pinus nigra* Mill.) with understory of oaks (*Quercus ilex* subsp. *rotundifolia*, *Quercus coccifera*, *Quercus faginea*), junipers (*Juniperus oxycedrus*), boxwood (*Buxus sempervirens*), rosemary (*Rosmarinus officinalis*), and thymes (*Thymus vulgaris*).

2.2. UAV data acquisition and processing

A fixed-wing UAV (eBee Classic of SenseFly) equipped with two optical sensors (RGB and multispectral) was used in this study (Fig. 2). The RGB camera was a SONY WX camera of 18.2 MP resolution and the multispectral sensor (MS) was a Parrot Sequoia of 1.2 MP single band resolution with a sunshine sensor and capable of recording surface reflectance in the green (550 nm ± 40 nm), red (660 nm ± 40 nm), red edge (735 nm ± 10 nm), and near infrared (790 nm ± 40 nm) spectral bands. A total of 49 flight campaigns were conducted between June and October 2021 over 82 plots, resulting in 12,007 individual images processed. Each cam-

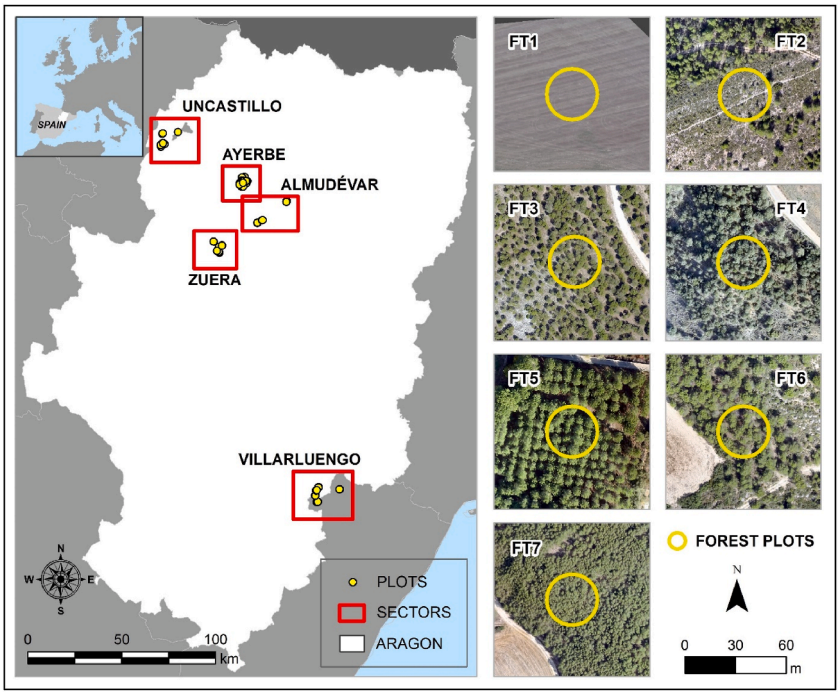

Fig. 1. Study area and examples of seven circular plots, one for each Prometheus fuel type.

Table 1
Summary of the forest plots and their associated Prometheus fuel types.

	FT1	FT2	FT3	FT4	FT5	FT6	FT7
Number of plots	10	11	8	7	10	13	23

Fig. 2. Above: (a) Main materials used in this study: SenseFly eBee Classic UAV unit with SONY WX camera and Parrot Sequoia multispectral sensor. Below: Examples of the same single image captured by the UAV in different spectral bands: (b) RGB; (c) Green band; (d) Red band; (e) Red edge band; and (f) Near infrared band. (For interpretation of the references to colour in this figure legend, the reader is referred to the Web version of this article.)

paign included two flights, one for each sensor attached to the UAV, making a total of 98 flights. All of them were automated using eMotion v.3.5.0 software, with specified parameters including a serpentine mapping, a flight altitude of 116.5 m from the ground, an angle of incidence of 90°, and an overlap between photographs of 90%–80% (cross- and along-track, respectively). Radiometric calibration was performed on the multispectral sensor to adjust it to the prevailing light conditions. For this, we followed the manufacturer-recommended method, combining the use of a reference panel and the sunshine sensor for calibrating the images. According to **Poncet et al. (2019)**, this procedure can be comparable to empirical calibration methods. Thus, we took four pictures of an Airinov calibration reference panel of known reflectance with the Parrot Sequoia camera prior to the start of each flight, while the sunshine sensor captured the current light conditions during the flights. The spatial resolutions of the RGB and multispectral images were 4 cm/px and 12 cm/px, respectively. Finally, in each flight area, at least four ground control points (GCPs) were measured with the Leica VIVA® GS15 CS10 GNSS. This allowed georeferencing the UAV images at centimetric scale to the ETRS89 UTM 30N reference system, while the vertical coordinates were converted from WGS84 ellipsoidal heights to EGM-96 geoidal heights model.

The data collected were processed using PIX4Dmapper v.4.5.6 software to obtain structural metrics, textural features, and spectral vegetation indices (Fig. 3). Multispectral images, captured with the Parrot Sequoia camera, were automatically calibrated by the PIX4Dmapper software during data processing (**Poncet et al., 2019**). Structural data were obtained from photogrammetric point clouds using "Structure from Motion" and stereo-matching algorithms included in PIX4Dmapper. These algorithms enabled image alignment and multi-view stereo reconstruction by detecting and matching image feature points in the acquired highly overlapping images (**Domingo et al., 2019**). Two photogrammetric point cloud datasets were generated, one for each sensor, with a higher average density in the RGB point clouds (3000 points/m^2) than in the multispectral point clouds (85 points/m^2). The "lidR" package (**Roussel et al., 2020**) for R environment v.4.2.0 (**R Core Team, 2022**) was used to clip both point cloud datasets in each forest plot and normalize their absolute heights. Normalization was performed using alternatively Digital Elevation Models (DEMs) with spatial resolutions of 0.5, 1, and 2 m, to examine the effect of DEM resolution on the accuracy of estimated heights and classification of forest fuels. DEMs were obtained from public ALS data from the PNOA project (Spanish National Aerial Orthophotography Plan). Noise and overlapping returns were removed, and ground points were classified following **Montealegre et al. (2016)** using the MCC-LiDAR v.2.1 command line tool (**Evans and Hudak, 2007**). The ground points were then interpolated using a TIN-to-Raster method (**Renslow, 2013**) to create the final DEMs. From the normalized UAV point clouds, a set of structural and textural variables was generated. Forest structural metrics were extracted at plot scale using FUSION/LDV v.4.21 software (**McGaughey, 2021**). They were related to height distribution (i.e., the minimum, mean and maximum elevation, and different height percentiles: P01, P05, P10 …. P99), height variability (i.e., the coefficient of variation, kurtosis, skewness, standard deviation, and variance of the heights), and canopy cover density (i.e., statistics of the returns at different height strata: 0.6, 2 and 4 m). Textural features were calculated from

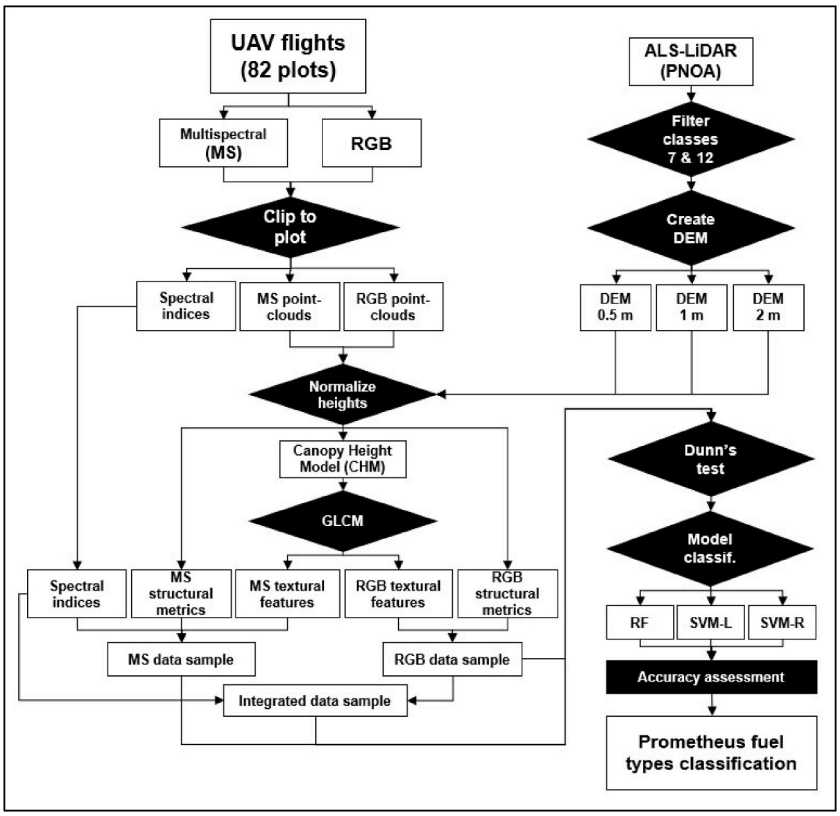

Fig. 3. Methodological scheme of the study.

the gray-level co-occurrence matrix (GLCM) (Haralick et al., 1973), using the "glcm" package for R environment (Zvoleff, 2020). GLCM were applied to previously created Canopy Height Models (CHM) in each plot using the "rasterize_canopy" function of the "lidR" package. Different window sizes were tested (3x3, 5x5, 7x7, and 9x9), with the 3x3 window providing the best results. Then, the mean values of four different offsets (0°, 45°, 90°, 135°) were analyzed and seven textural features were extracted at the three spatial resolutions of the DEM (contrast, dissimilarity, entropy, homogeneity, mean, second moment, and variance). Finally, four zonal statistics were calculated for each plot-scale metric (minimum, maximum, mean, and median).

In addition, seven spectral vegetation indices were calculated from reflectance data of multispectral images: the Advanced Vegetation Index (AVI) (Equation (1); Roy et al., 1996), the Green Chlorophyll Index (GCI) (Equation (2); Gitelson et al., 2003), the Green Normalized Difference Vegetation Index (GNDVI) (Equation (3); Gitelson et al., 1996), the Normalized Difference Red Edge Index (NDRE) (Equation (4); Barnes et al., 2000), the Normalized Difference Vegetation Index (NDVI) (Equation (5); Rouse et al., 1974), the Normalized Difference Water Index (NDWI) (Equation (6); Gao, 1996), and the Soil Adjusted Vegetation Index (SAVI) (Equation (7); Huete, 1988). For each of the seven indices, the same four zonal statistics at plot scale as in the textural metrics were calculated.

$$AVI = [NIR \times (255 - R) \times (NIR - R)]^{1/3} \quad (1)$$

$$GCI = \left(\frac{NIR}{G}\right) - 1 \quad (2)$$

$$GNDVI = \frac{NIR - G}{NIR + G} \quad (3)$$

$$NDRE = \frac{NIR - RedEdge}{NIR + RedEdge} \quad (4)$$

$$NDVI = \frac{NIR - R}{NIR + R} \quad (5)$$

$$NDWI = \frac{G - NIR}{G + NIR} \quad (6)$$

$$SAVI = \frac{(1 + L) \times (NIR - R)}{NIR + R + L} \quad (L = 0.5) \quad (7)$$

Where NIR is near infrared band, R is red band, G is green band, RedEdge is red edge band.

2.3. Prometheus fuel types classification and model validation

A total of 138 variables were generated for input into the classification models, which included 82 structural metrics, 28 textural features, and 28 spectral indices. The post hoc non-parametric Dunn's test of multiple comparison was used to select the most relevant variables. This method is similar to Kruskal-Wallis test but with the ability to determine the groups that are statistically different for the classification of forest attributes on machine learning models (García-Galar et al., 2023). From each of the three groups of variables, including the three subgroups of structural metrics, we finally selected those with a high ability to differentiate between the pairs for input into the classification models.

Three different data samples were tested: the relevant structural and textural variables from the RGB sensor (RGB data sample), the relevant structural, textural, and spectral variables from the multispectral sensor (MS data sample), and the relevant structural and textural variables from the RGB sensor combined with the relevant spectral variable from the multispectral sensor (integrated data sample). For each of these three data samples, the three normalized point cloud datasets from the different DEM resolutions were tested, totalizing 9 data samples to introduce into the classification models. Three non-parametric predictive models were then tested through the "caret" package (Kuhn, 2008) for R environment: Random Forest (RF) and Support Vector Machine with both linear (SVM-L) and radial (SVM-R) kernels. RF classifiers were parametrized by applying between 2 and 10 decision trees at each node and SVM models were fitted by applying a cost parameter within the interval 1-1000. Models were validated using the k-fold cross-validation method, recommended for small datasets (Anderson et al., 2005), testing in groups of 5 and 10 observations, and 10, 50, and 100 repeats in each case. Finally, the most accurate data sample, model, and validation method was assessed based on the overall accuracy (OA) coefficient and the producer's and user's accuracies of the confusion matrices, which are determined by the commission and omission errors, respectively (Pontius et al., 2008).

3. Results

3.1. Most significant variables for the classification models

Dunn's test revealed the variables with the highest distinguishability among the 21 pairs of Prometheus fuel types. In general, Prometheus main fire carriers were well differentiated, while more difficulties were observed in fuels of the same dominant stratum. As shown in Fig. 4, a maximum of 109 variables were able to differentiate between the FT1-FT7, which was the peer group with the highest distinguishing ability. High differentiation abilities were also found between FT2-FT5 (84 variables), FT1-FT6 (83 variables), FT1-FT5 (80 variables), FT3-FT5 (66 variables), FT2-FT7 (69 variables), and FT2-FT6 (60 variables). The ability to differentiate between grassland and shrub fuel types was somewhat lower (FT1-FT2: 40 variables; FT1-FT3: 29 variables; FT1-FT4: 35 variables). As for differentiation within tree fuel types, 39 variables differentiated between FT5-FT7, 9 variables between FT5-FT6, and only 2 vari-

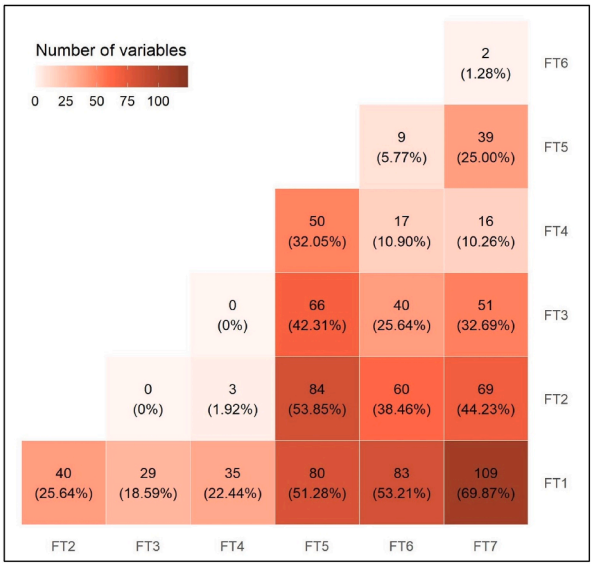

Fig. 4. Number of variables and percentage with respect to the total of variables able to differentiate the 21 pairs of Prometheus fuel types according to Dunn's test.

ables between FT6-FT7. Finally, only 3 variables differentiated between FT2-FT4 shrub fuel types, and none of them distinguished between FT2-FT3 and FT3-FT4.

Out of the three sub-groups of structural metrics, 9 variables related to vegetation height distribution were able to differentiate up to 11 pairs of fuel types, the coefficient of variation from the height variability subgroup distinguished 9 pairs, and 6 variables related to the canopy cover density were able to discern up to 12 pairs. In addition, 6 variables from the textural features statistics were able to distinguish up to 7 pairs, and 12 variables from the spectral indices statistics distinguished a maximum of 7 pairs. All relevant variables are shown in Table 2 and full results are described in Table S1 of the Supplementary Materials.

Based on the results obtained and in order to generate parsimonious models after testing different combinations, the variables selected from each group for inclusion in the classification models were the vegetation height at the 50th percentile, the coefficient of variation of the heights, the percentage of returns above 4 m, the mean dissimilarity, and the mean of the Green Chlorophyll Index (Table 3).

3.2. *Performance of prometheus fuel types classification*

The best performing models were obtained systematically using the integrated data sample and the RF classification method (Table 4). Overall, best k-fold cross validation method was obtained with 10 observations and 10 repeats in each case. The SVM-L and SVM-R models had significantly lower accuracies in all cases (see Tables S2 and S3 of the Supplementary Materials). The best classification of the Prometheus fuel types was reached with the point cloud normalized to the DEM of 0.5 m resolution, yielding an OA of

Table 2
Relevant variables for their high ability to distinguish between pairs of Prometheus fuel types according to Dunn's test.

Groups of variables	Variables	Maximum number of pairs able to differentiate
Height distribution	Elev. maximum, Elev. P50 – Elev. P99	11
Height variability	Elev. CV	9
Canopy cover density	Elev. strata >4 m: max, mean, median, mode, return proportion; Percentage of returns >4 m	12
Textural features	GLCM dissimilarity: mean; GLCM mean: max, median, min; GLCM variance: max, min	7
Spectral indices	GCI: max, mean, median; GNDVI: max, median; NDRE: max; NDVI: max, mean, median; NDWI: median, mean; SAVI: max	7

Table 3
Final variables introduced in the classification models.

Groups of variables	Variable	Description
Height distribution	Elev. P50	Vegetation height at the 50th percentile
Height variability	Elev. CV	Coefficient of variation of the heights
Canopy cover density	Percentage of returns >4 m	Percentage of returns above 4 m
Textural features	GLCM dissimilarity mean	Mean dissimilarity
Spectral indices	GCI mean	Mean of the Green Chlorophyll Index

Table 4
Summary of overall accuracies of Prometheus fuel types classification for the nine RF model data samples with k-10 cross validation and 10 repeats in each case.

DEM resolution	Data sample	Overall Accuracy
0.5 m	RGB	63%
	MS	66%
	Integrated	71%
1 m	RGB	64%
	MS	61%
	Integrated	70%
2 m	RGB	59%
	MS	62%
	Integrated	65%

71%. When the MS data sample was introduced, the best OA was 7.58% lower than the integrated data sample (OA = 66%) using the same DEM resolution to normalize the point cloud. The best OA of the RGB data sample was 10.94% and 3.13% lower than the integrated and MS data samples, respectively (OA = 64%), in this case with the point cloud normalized to the DEM of 1 m resolution, although the classification with the 0.5 DEM had very similar accuracies (OA = 63%) (Table 4).

The confusion matrix of the best model shows the classification accuracy of each of the 7 Prometheus fuel types (Table 5). FT1 had the best hit rate, with a 98% of producer's accuracy and 83% of user's accuracy. FT2 and FT7 were the types with the best hit rate among the shrub and tree types, respectively, followed by FT4 and FT5. On the other hand, the highest confusion rates were found in FT3 and FT6. In general, confusions occurred between fuel types of the same main fire carrier, with some exceptions. For instance, a high percentage of FT3 plots were misclassified as FT2 and some as FT4, although commission errors due to incorrect classification in grasslands (FT1) were also found. Regarding confusion in FT6, many plots were misclassified as FT7 and, to a lesser extent, FT5, with no errors outside of tree fuel types. The main confusion between fuel types of different strata occurred between FT4 and FT7 (dense shrub and tree fuel types, respectively), and there were a few omission errors in FT1 due to misclassifications in FT3 and FT4. Regarding confusion matrices of the best MS and RGB data samples (Tables S4 and S5 of the Supplementary Materials), more confusion rates were observed in all fuel types, but still, very few errors were found between the different strata.

The percentage of hits and misclassification errors in the fuel types can be explained by observing the distribution values of the five variables of the classification models, as shown in Fig. 5. Both the three shrub and the three tree fuel types present similar patterns that, in general, make their correct differentiation difficult. The values of FT1 (grassland fuel type) are quite different from the rest, which explains the high percentages of success obtained in their classification. The values of the shrub and tree fuel types are very different from each other, although they present a similar distribution in the GCI spectral index. Thus, confusions within types of the same stratum are to be expected, since their distribution values are similar, especially between FT2-FT3 in the three structural variables. In the tree types, the FT5 and FT7 values of the structural and spectral variables are distributed differently, while FT6 values overlap with those of FT5 and FT7, which explains the greater confusion in this type compared to the other two.

4. Discussion

UAV-derived photogrammetric point clouds and multispectral indices allowed classifying fuel types in the Prometheus scale with good levels of accuracy, with most of the confusions found in types belonging to the same dominant stratum. Our results suggest that the combined use of RGB and multispectral data is the best option to classify fuel types. Furthermore, better classifications were observed when using the point cloud normalized to the DEM of 0.5 m resolution and when classifying with RF, which proved to be substantially better than SVM-L and SVM-R. The main fire carriers were well distinguished, and confusions were observed mainly within the three shrub and tree fuel types, especially in the shrub strata.

The integrated data sample obtained the best results in the classification models, reaching accuracies similar to those of **Marino et al. (2016)**, who used ALS-LiDAR, Landsat-8 OLI multispectral imagery, and decision-based algorithms to classify specific Canary Island fuel types (OA = 70%). **Domingo et al. (2020)** obtained lower accuracies when classifying Prometheus fuel types in Mediterranean forest stands using low-density ALS-LiDAR and Sentinel-2 imagery by means of machine learning. However, they got better accuracies with SVM-R (OA = 59%) than RF (OA = 56%). We assume that the better performance of the integrated data sample was

Table 5
Confusion matrix of the best model (RF, integrated data sample, and point-cloud normalized at 0.5 m DEM resolution) for Prometheus fuel types classification.

Fuel type	FT1	FT2	FT3	FT4	FT5	FT6	FT7	User's accuracy
FT1	**98**	0	10	10	0	0	0	83%
FT2	2	**90**	37	0	0	0	0	70%
FT3	0	16	**31**	10	0	0	0	54%
FT4	0	4	2	**47**	0	0	9	76%
FT5	0	0	0	0	**73**	29	10	65%
FT6	0	0	0	0	17	**54**	29	54%
FT7	0	0	0	3	10	37	**192**	79%
Prod.'s accuracy	98%	82%	39%	67%	73%	45%	80%	

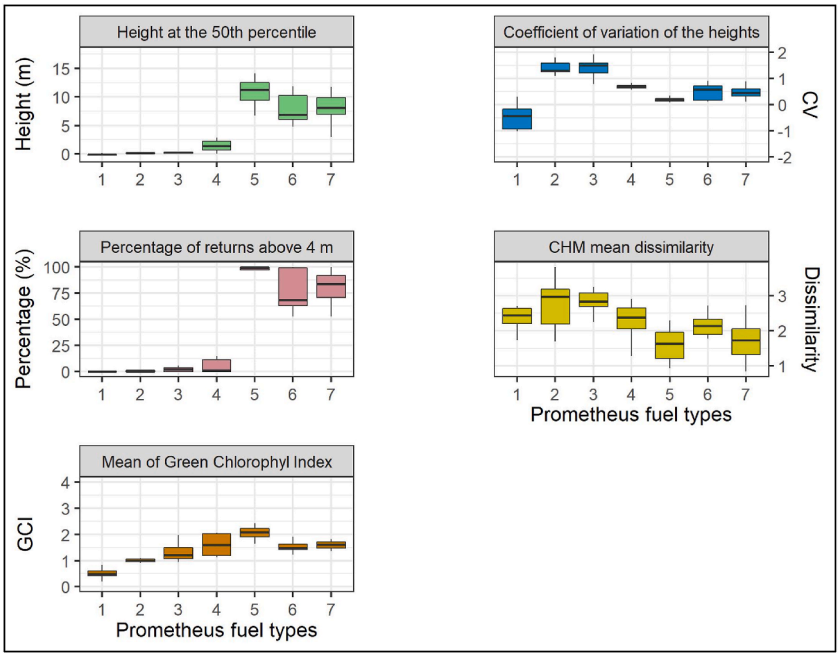

Fig. 5. Distribution values of the five UAV variables introduced into the classification models for the identification of the Prometheus fuel types.

due to the higher average of the point clouds from RGB images compared to the point clouds of the multispectral images, which allowed for more normalized point heights and consequently more accurate structural and textural variables. Kandare et al. (2016) also found higher accuracy in individual tree crowns delineation with higher ALS point cloud density, and Ruiz et al. (2014) achieved better correlation values in forest attributes prediction with high LiDAR data density. In addition, Domingo et al. (2019) obtained better accuracies when using UAV photogrammetric point clouds derived from RGB cameras than from multispectral sensors. Our integrated data sample used both RGB and multispectral data, which could imply a higher time cost in data acquisition when these sensors cannot collect information simultaneously, requiring two flights of the UAV, as in our case. Accuracies for the MS data sample were lower than for the integrated data sample due to the lower density of the point cloud, and confusions between fuel types were higher in all cases. Here, the OA was higher when the 0.5 m resolution DEM was used to normalize the point clouds, underscoring the importance of using fine-scale DEMs for this purpose, as noted by other authors (e.g., Cao et al., 2019; Shin et al., 2018).

The confusion matrices indicated the presence of significant misclassification error rates between fuel types belonging to the same main fire carrier (i.e., within the three shrub fuel types and the three tree fuel types). According to the results of the Dunn's test, only 3 variables were able to distinguish between FT2-FT4 and none were able to distinguish between the others two pairs of shrub fuel types. There were also few variables capable of distinguishing between the tree types. These confounds were to be expected, as there are no absolutely unequivocal plots in terms of fuel type, even though we worked on plots as homogeneous as possible for each type in order to avoid confusion. However, this may also indicate a limitation of optical UAVs to differentiate between similar fuel types, given the inability of photogrammetric point clouds to penetrate the canopy. Therefore, medium to high confusion among shrub fuels can be expected when using optical UAVs, especially in the closest types (FT2-FT3 and FT3-FT4), since they present few differences in terms of height criteria and similar features. The same is true for the confusion observed between tree types. In contrast, no significant problems were observed between the fuel types of different main fire carriers, except for FT4-FT7, which has also been noted using ALS-LiDAR data (Domingo et al., 2020). This confusion is due to the high density of understory and canopy and the vertical continuity of the fuel in both types. The low capability of optical UAVs to collect fuel information in medium and low strata could be overcome by using LiDAR UAVs (e.g., Dalla Corte et al., 2020; Neuville et al., 2021), although their economic costs are considerably high. However, previous work related to forest structure estimation and mapping have obtained successful results using photogrammetric point clouds (e.g., Carbonell-Rivera et al., 2022; Shin et al., 2018). Additionally, Wallace et al. (2016) and Cao et al. (2019) shown that UAV-derived photogrammetric point clouds can be useful and effective substitutes for UAV-LiDAR point clouds for estimating structural attributes of forests. Based on the results obtained in this study, optical UAVs can be considered as suitable alternatives to ALS-LIDAR systems, especially ALS flights of systematic coverage for large extensions carried out by public or private initiatives, whose point density is usually low. In this sense, the higher point density that can be obtained with optical UAVs compared to these low-density ALS flights may allow a better characterization of vegetation structure and forest fuels at local or regional scales. In addition, UAV data can be obtained on demand, allowing for greater temporal flexibility. Photogrammetric point clouds can also be integrated with ALS data to reduce misclassification errors in fuel types and improve their classification (e.g., Guerra-Hernández et al., 2018; Yoshii et al., 2022). Another option to improve the classification could be to fuse canopy information from photogram-

metric point clouds with understory data collected from terrestrial or mobile laser scanners (e.g., Brede et al., 2022; Panagiotidis et al., 2022).

Regarding the multispectral indices, the Parrot Sequoia camera has proven to be able to capture the state of the vegetation (i.e., healthy or diseased). Previous studies have reported good overall performance for this camera. For instance, Fawcett et al. (2020) compared vegetation indices generated by Parrot Sequoia camera, HyPlant airborne imaging spectrometer and Sentinel-2 imagery, showing overall good agreement, although some bias was noticed in the Parrot Sequoia camera for high and low reflective surface. Lu et al. (2020) demonstrated that the Parrot Sequoia offered similar performance to the DJI Phantom 4 multispectral camera, despite having different spectral response functions, and that both accurately estimated NDVI when compared to spectroradiometer recordings. However, Pérez-Cardiel et al. (2022) found that the Parrot Sequoia had some underestimates in the red edge band and small overestimates in the NIR band when compared to spectroradiometer records and Sentinel-2 images. Additionally, Stow et al. (2019) observed slightly lower reflectance in the NIR band of the Parrot Sequoia around solar noon and noted the contrast between the shadowed and illuminated areas in all spectral bands. Therefore, some uncertainty must be assumed in the data recorded by our multispectral sensor.

5. Conclusions

The identification of forest fuels is an important step for the prevention and mitigation of wildfires, as it allows forest managers to understand the behavior and intensity of fire in a forest stand. This study used imagery from a fixed-wing UAV to derive a set of structural, textural, and spectral variables, which have been capable of classifying the Prometheus fuel models in Mediterranean forest environments with good levels of agreement. However, more research is needed to understand the capabilities and limitations of these promising instruments. The results obtained allow validating optical UAVs as affordable tools to identify and monitor forest fuels at a local and regional scale and contribute to the successful prevention of forest fires in Mediterranean ecosystems.

Funding

This work was supported by the Spanish Ministry of Science, Innovation, and Universities through an FPU predoctoral contract granted to R.H. (FPU18/05027); and by the Government of Aragon (Geoforest S51_20R co-financed with FEDER "Construyendo Europa desde Aragón").

Author statement

R. Hoffrén: Conceptualization, Methodology, Software, Validation, Formal Analysis, Investigation, Data Curation, Writing – Original Draft, Writing – Review & Editing. **M.T. Lamelas:** Conceptualization, Methodology, Validation, Investigation, Writing – Original Draft, Writing – Review & Editing. **J. de la Riva:** Conceptualization, Methodology, Validation, Investigation, Writing – Original Draft, Writing – Review & Editing.

Ethical Statement

Hereby, I Raúl Hoffrén consciously assure that for the manuscript "UAV-derived photogrammetric point clouds and multispectral indices for fuel estimation in Mediterranean forests" the following is fulfilled:

1) This material is the authors' own original work, which has not been previously published elsewhere.
2) The paper is not currently being considered for publication elsewhere.
3) The paper reflects the authors' own research and analysis in a truthful and complete manner.
4) The paper properly credits the meaningful contributions of co-authors and co-researchers.
5) The results are appropriately placed in the context of prior and existing research.
6) All sources used are properly disclosed (correct citation). Literally copying of text must be indicated as such by using quotation marks and giving proper reference.
7) All authors have been personally and actively involved in substantial work leading to the paper, and will take public responsibility for its content.

The violation of the Ethical Statement rules may result in severe consequences.

To verify originality, your article may be checked by the originality detection software iThenticate. See also http://www.elsevier.com/editors/plagdetect.

I agree with the above statements and declare that this submission follows the policies of Solid State Ionics as outlined in the Guide for Authors and in the Ethical Statement.

Declaration of competing interest

The authors declare that they have no known competing financial interests or personal relationships that could have appeared to influence the work reported in this paper.

Data availability

Data will be made available on request.

Appendix A. Supplementary data

Supplementary data to this article can be found online at https://doi.org/10.1016/j.rsase.2023.100997.

References

Albini, F., 1976. Estimating wildfire behavior and effects. In: USDA Forest Service, Intermountain Forest and Range Experiment Station, General Technical Report INT, 30, p. 92.

Anderson, H.E., McGaughey, R.J., Reutebuch, S.E., 2005. Estimating forest canopy fuel parameters using LiDAR data. Remote Sens. Environ. 94 (4), 441–449. https://doi.org/10.1016/j.rse.2004.10.013.

Barnes, E.M., Clarke, T.R., Richards, S.E., 2000. Coincident detection of crop water stress, nitrogen status and canopy density using ground-based multispectral data. In: Proceedings of the 5th International Conference on Precision Agriculture and Other Resource Managements. July 16–19, 2000, Bloomington, MN, USA.

Brede, B., Terryn, L., Barbier, N., Bartholomeus, H.M., Bartolo, R., Calders, K., Derroire, G., Moorthy, S.M.K., Lau, A., Levick, S.R., Raumonen, P., Verbeeck, H., Wang, D., Whiteside, T., van der Zee, J., Herold, M., 2022. Non-destructive estimation of individual tree biomass: allometric models, terrestrial and UAV laser scanning. Remote Sens. Environ. 280, 113180. https://doi.org/10.1016/j.rse.2022.113180.

Cao, L., Liu, H., Fu, X., Zhang, Z., Shen, X., Ruan, H., 2019. Comparison of UAV LiDAR and Digital Aerial Photogrammetry point clouds for estimating forest structural attributes in subtropical planted forests. Forests 10 (2), 145. https://doi.org/10.3390/f10020145.

Carbonell-Rivera, J.P., Torralba, J., Estornell, J., Ruiz, L.A., Crespo-Peremarch, P., 2022. Classification of Mediterranean shrub species from UAV point clouds. Rem. Sens. 14, 199. https://doi.org/10.3390/rs14010199.

Dalla Corte, A.P., Rex, F.E., Alves de Almeida, D.R., Sanquetta, C.R., Silva, C.A., Moura, M.M., Wilkinson, B., Almeyda Zambrano, A.M., da Cunha Neto, E.M., Veras, H.F.P., de Moraes, A., Klauberg, C., Mohan, M., Cardil, A., Broadbent, E.N., 2020. Measuring individual tree diameter and height using GatorEye high-density UAV-LiDAR in an integrated crop-livestock-forest system. Rem. Sens. 12 (5), 863. https://doi.org/10.3390/rs12050863.

Domingo, D., Orka, H.Ø., Næsset, E., Kachamba, D., Gobakken, T., 2019. Effects of UAV image resolution, camera type, and image overlap on accuracy of biomass predictions in a tropical woodland. Rem. Sens. 11, 948. https://doi.org/10.3390/rs11080948.

Domingo, D., de la Riva, J., Lamelas, M.T., García-Martín, A., Ibarra, P., Echeverría, M., Hoffrén, R., 2020. Fuel type classification using airborne laser scanning and sentinel 2 data in Mediterranean forest affected by wildfires. Rem. Sens. 12 (21), 1–22. https://doi.org/10.3390/rs12213660.

Evans, J.S., Hudak, A.T., 2007. A multiscale curvature algorithm for classifying discrete return LiDAR in forested environments. IEEE Trans. Geosci. Rem. Sens. 45 (4), 1029–1038. https://doi.org/10.1109/TGRS.2006.890412.

Fawcett, D., Panigada, C., Tagliabue, G., Boschetti, M., Celesti, M., Evdokimov, A., Biriukova, K., Colombo, R., Miglietta, F., Rascher, U., Anderson, K., 2020. Multi-scale evaluation of drone-based multispectral surface reflectance and vegetation indices in operational conditions. Rem. Sens. 12 (3), 514. https://doi.org/10.3390/rs12030514.

Fernández-Álvarez, M., Armesto, J., Picos, J., 2019. LiDAR-based wildfire prevention in WUI: the automatic detection, measurement and evaluation of forest fuels. Forests 10, 148. https://doi.org/10.3390/f10020148.

Ferraz, A., Saatchi, S., Mallet, C., Meyer, V., 2016. Lidar detection of individual tree size in tropical forests. Remote Sens. Environ. 183, 318–333. https://doi.org/10.1016/J.RSE.2016.05.028.

Fritz, A., Kattenborn, T., Koch, B., 2013. UAV-based photogrammetric point clouds – tree stem mapping in open stands in comparison to terrestrial laser scanner point clouds. ISPRS Int. Arch. Photogram. Rem. Sens. Spatial Inf. Sci. XL-1/W2, 141–146. https://doi.org/10.5194/isprsarchives-XL-1-W2-141-2013.

García-Galar, A., Lamelas, M.T., Domingo, D., 2023. Assessment of oak groves conservation statuses in Natura 200 sacs with single photon LiDAR and Sentinel-2 data. Rem. Sens. 15, 710. https://doi.org/10.3390/rs15030710.

Gao, B.C., 1996. NDWI – a Normalized Difference Water Index for remote sensing of vegetation liquid water from space. Remote Sens. Environ. 58 (3), 257–266. https://doi.org/10.1016/S0034-4257(96)00067-3.

Gitelson, A.A., Gritz, Y., Merzlyak, M.N., 2003. Relationships between leaf chlorophyll content and spectral reflectance and algorithms for non-destructive chlorophyll assessment in higher plant leaves. J. Plant Physiol. 160, 271–282. https://doi.org/10.1078/0176-1617-00887.

Gitelson, A.A., Kaufman, Y.J., Merzlyak, M.N., 1996. Use of a green channel in remote sensing of global vegetation from EOS-MODIS. Remote Sens. Environ. 58, 289–298. https://doi.org/10.1016/S0034-4257(96)00072-7.

Guerra-Hernández, J., Cosenza, D.N., Rodriguez, L.C.E., Silva, M., Tomé, M., Díaz-Varela, R.A., González-Ferreiro, E., 2018. Comparison of ALS- and UAV(SfM)-derived high-density point clouds for individual tree detection in Eucalyptus plantations. Int. J. Rem. Sens. 39 (15–16), 5211–5235. https://doi.org/10.1080/01431161.2018.1486519.

Haralick, R.M., Shanmugam, K., Dinstein, I., 1973. Textural features for image classification. IEEE Trans. Syst. Man Cybern. Syst. 3 (6), 610–621. https://doi.org/10.1109/TSMC.1973.4309314.

Hillman, S., Wallace, L., Lucieer, A., Reinke, K., Turner, D., Jones, S., 2021. A comparison of terrestrial and UAS sensors for measuring fuel hazard in a dry sclerophyll forest. Int. J. Appl. Earth Obs. Geoinf. 95, 102261. https://doi.org/10.1016/j.jag.2020.102261.

Huete, A.R., 1988. A soil-adjusted vegetation index (SAVI). Remote Sens. Environ. 25, 295–309. https://doi.org/10.1016/0034-4257(88)90106-X.

Kandare, K., Orka, H.Ø., Cheung-Wai Chan, J., Dalponte, M., 2016. Effects of forest structure an airborne laser scanning point cloud density on 3D delineation of individual tree crowns. Eur. J. Remote Sens. 49, 337–359. https://doi.org/10.5721/EuJRS20164919.

Kuhn, M., 2008. Building predictive models in R using the caret package. J. Stat. Software 28 (5), 1–26. https://doi.org/10.18637/jss.v028.i05.

Lu, H., Fan, T., Ghimire, P., Deng, L., 2020. Experimental evaluation and consistency comparison of UAV multispectral minisensors. Rem. Sens. 12 (16), 2542. https://doi.org/10.3390/rs12162542.

Marino, E., Ranz, P., Tomé, J.L., Noriega, M.Á., Esteban, J., Madrigal, J., 2016. Generation of high-resolution fuel model maps from discrete airborne laser scanner and Landsat-8 OLI: a low-cost and highly updated methodology for large areas. Remote Sens. Environ. 187, 267–280. https://doi.org/10.1016/j.rse.2016.10.020.

McGaughey, R.J., 2021. FUSION/LDV: Software for LIDAR Data Analysis and Visualization V.4.21. USDA Forest Service, Washington DC, USA.

Messinger, M., Asner, G., Silman, M., 2016. Rapid assessments of Amazon forest structure and biomass using small unmanned aerial systems. Rem. Sens. 8, 615. https://doi.org/10.3390/rs8080615.

Montealegre, A.L., Lamelas, M.T., de la Riva, J., García-Martín, A., Escribano, F., 2016. Use of low point density ALS data to estimate stand-level structural variables in Mediterranean Aleppo pine forest. Forestry 89, 373–382. https://doi.org/10.1093/forestry/cpw008.

Neuville, R., Bates, J.S., Jonard, F., 2021. Estimating forest structure from UAV-mounted LiDAR point cloud using machine learning. Rem. Sens. 13 (3), 352. https://doi.org/10.3390/rs13030352.

Oliveira, S., Oehler, F., San Miguel-Ayanz, J., Camia, A., Pereira, J.M.C., 2012. Modeling spatial patterns of fire occurrence in mediterranean Europe using multiple regression and random forest. For. Ecol. Manag. 275, 117–129. https://doi.org/10.1016/j.foreco.2012.03.003.

Panagiotidis, D., Abdollahnejad, A., Slavík, M., 2022. 3D point cloud fusion from UAV and TLS to assess temperate managed forest structures. Int. J. Appl. Earth Obs. Geoinf. 112, 102917. https://doi.org/10.1016/j.jag.2022.102917.

Pérez-Cardiel, E., de la Riva, J., Rodrigues, M., Domingo, D., Casterad, M.A., 2022. Evaluación de la consistencia de los datos obtenidos desde UAV por el sensor Sequoia para su aplicación en agricultura. In: Ruiz, L.A., Estornell, J., González-Audícana, M., Álvarez-Mozos, J. (Eds.), Teledetección para una agricultura sostenible en la era del Big Data. XIX Congreso de la Asociación Española de Teledetección. Pamplona. eISBN: 978-84-9769-383-7.

Poncet, A.M., Knappenberger, T., Brodbeck, C., Fogle, Jr, M., Shaw, J.N., Ortiz, B.V., 2019. Multispectral UAS data accuracy for different radiometric calibration methods. Rem. Sens. 11 (16), 1917. https://doi.org/10.3390/rs11161917.

Pontius, R.G., Boersma, W., Castella, J.C., Clarke, K., de Nijs, T., Dietzel, C., Duan, Z., Fotsing, E., Goldstein, N., Kok, K., Koomen, E., Lippitt, C.D., McConnell, W., Sood, A.M., Pijanowski, B., Pithadia, S., Sweeney, S., Trung, T.N., Veldkamp, A.T., Verburg, P.H., 2008. Comparing the input, output, and validation maps for several models of land change. Ann. Reg. Sci. 42, 11–37. https://doi.org/10.1007/s00168-007-0138-2.

Prometheus, 1999. Management Techniques for Optimization of Suppression and Minimization of Wildfires Effects. System Validation. European Commission, DG XII,

ENVIR & CLIMATE. European Commission, Luxembourg. Contract Number ENV4–CT98–0716.
Puliti, S., Olerka, H., Gobakken, T., Naesset, E., 2015. Inventory of small forest areas using an unmanned aerial system. Rem. Sens. 7, 9632–9654. https://doi.org/10.3390/rs70809632.
R Core Team, 2022. R: A Language and Environment for Statistical Computing. R Foundation for Statistical Computing, Vienna, Austria. URL. https://www.R-project.org/.
Renslow, M., 2013. Manual of Airborne Topographic Lidar. ASPRS, Bethesda, MD. ISBN: 978-1570830976.
Rothermel, C., 1972. A Mathematical Model for Predicting Fire Spread in Wildland Fuels. Research Papers, INT-115. U.S. Department of Agriculture, Intermountain Forest and Range Experiment Station, Ogden, UT, p. 40.
Rouse, J.W., Haas, R.H., Schell, J.A., Deering, D.W., 1974. Monitoring Vegetation Systems in the Great Plains with ERTS. Third ERTS-1 Symposium NASA, NASA SP-351, Washington DC, pp. 309–317.
Roussel, J.R., Auty, D., Coops, N.C., Tompalski, P., Goodbody, T.R.H., Sánchez-Meador, A., Bourdon, J.F., de Boissieu, F., Achim, A., 2020. lidR: an R package for analysis of Airborne Laser Scanning (ALS) data. Remote Sens. Environ. 251, 112061. https://doi.org/10.1016/j.rse.2020.112061.
Roy, P.S., Sharma, K.P., Jain, A., 1996. Stratification of density in dry deciduous forest using satellite remote sensing digital data – an approach based on spectral indices. J. Biosci. 21 (5), 723–734. https://doi.org/10.1007/BF02703148.
Ruiz, L.A., Hermosilla, T., Mauro, F., Godino, M., 2014. Analysis of the influence of plot size and LiDAR density on forest structure attribute estimates. Forests 5 (5), 936–951. https://doi.org/10.3390/f5050936.
Shin, P., Sankey, T., Moore, M.M., Thode, A.E., 2018. Evaluating unmanned aerial vehicle images for estimating forest canopy fuels in a Ponderosa pine stand. Rem. Sens. 10, 1266. https://doi.org/10.3390/rs10081266.
Stow, D., Nichol, C.J., Wade, T., Assmann, J.J., Simpson, G., Helfter, C., 2019. Illumination geometry and flying height influence surface reflectance and NDVI derived from multispectral UAS imagery. Drones 3 (3), 55. https://doi.org/10.3390/drones3030055.
Varol, T., Canturk, U., Cetin, M., Ozel, H.B., Sevil, H., 2021. Impacts of climate scenarios on European ash tree (*Fraxinus excelsior* L.) in Turkey. For. Ecol. Manag. 491, 119199. https://doi.org/10.1016/j.foreco.2021.119199.
Venäläinen, A., Lehtonen, I., Laapas, M., Ruosteenoja, K., Tikkanen, O.L., Viiri, H., Ikonen, V.P., Peltola, H., 2020. Climate change induces multiple risks to boreal forests and forestry in Finland: a literature review. Global Change Biol. 26 (8), 4178–4196. https://doi.org/10.1111/gcb.15183.
Wallace, L., Lucieer, A., Malenovský, Z., Turner, D., Vopěnka, P., 2016. Assessment of forest structure using two UAV techniques: a comparison of Airborne Laser Scanning and Structure from Motion (SfM) point clouds. Forests 7 (3), 62. https://doi.org/10.3390/f7030062.
Yoshii, T., Matsumura, N., Lin, C., 2022. Integrating UAV-SfM and airborne lidar point cloud to plantation forest feature extraction. Rem. Sens. 14 (7), 1713. https://doi.org/10.3390/rs14071713.
Zvoleff, A., 2020. glcm: calculate textures from grey-level co-occurrence matrices (GLCMs). R package version 1.6.5. https://CRAN.R-project.org/package=glcm.